Science and Technology for Energy Transition **79**, 20 (2024)

https://doi.org/10.2516/stet/2024009

Decarbonizing Energy Systems: Smart Grid and Renewable Technologies
Fang Rui-ming and Qiangqiang Liao (Guest Editors)

Available online at:
stet-review.org

REGULAR ARTICLE OPEN ACCESS

Sliding mode sensorless control of wind turbine pitch motor with ESO feedforward compensation in the offshore wind power system

Dehai Chen[1], Jixiang Zhang[1], and Tian Zhang[2,*]

[1] School of Electrical Engineering and Automation, Jiangxi University of Science and Technology, No. 1958 Kejia Road, Nankang District, Ganzhou 341000, China
[2] Ganzhou Slon Magnetic Separator Co. Ltd, No. 6 Shahe Road, Zhanggong District, Ganzhou 341000, China

Received: 27 October 2023 / Accepted: 30 January 2024

Abstract. In order to improve the dynamic performance of the control system, a variable frequency sliding mode sensorless control strategy based on Extended State Observer (ESO) feedforward compensation was proposed in order to improve the disturbance and jitter problems of pitch motors in offshore wind power generation systems. The fast exponential reaching law is designed in the velocity loop, and the integrated sliding surface is adopted, which reduces the steady-state error of the traditional sliding surface and weakens the jitter phenomenon of the moving point on the sliding surface. The traditional sliding mode observer is improved, and the variable cut-off frequency filter is used instead of the low-pass filter in the filtering process to filter the signals of each speed band. At the same time, in order to estimate the disturbances in the system, the Linear Extended State Observer (LESO) is designed to observe and compensate for the unknown disturbances, which improves the robustness of the system. The simulation results show that the control strategy in this paper solves the problems of traditional Sliding Mode Control (SMC), which not only shortens the response time of the system, but also significantly improves the anti-disturbance performance of the system, and the overall effect is significantly improved.

Keywords: Change the cutoff frequency, Fast exponential reaching law, Extended State Observer, Sliding mode observe.

1 Introduction

Permanent Magnet Synchronous Motor (PMSM) has been widely used in many fields such as aerospace, servo systems, electric vehicles, and wind power generation due to its high efficiency, high power density, and wide speed regulation range. In the field of wind power generation, the pitch motor in the offshore wind power generation system, as a kind of PMSM, faces a more complex working environment. In order to improve the performance of pitch motors in offshore wind power generation systems, and improve the power efficiency of wind turbines, it is particularly important to improve the design of control systems [1–7].

The sensorless control technology of PMSMs can eliminate the traditional mechanical sensor, simplify the structure of the pitch motor control system, reduce the system cost, and further improve the system reliability. At present, there are several sensorless control methods: flux estimation method, sliding mode observer, high-frequency injection method, model reference adaptation, and extended Kalman filter. Since the existence of disturbances during the operation of PMSMs is unavoidable, the design of disturbance observers is also essential.

In the 1980s, Ohnishi, a Japanese scholar, was the first to apply disturbance observers to control systems. Since then, researchers have extensively studied and applied various types of disturbance observers. In the context of PMSMs, commonly used disturbance observers include Luenberger observers, Kalman filters, and extended state observers [8–11]. Reference [12], the extended state observer was employed to convert existing disturbances of the system into state variables and compensate for them in the controller, thereby enhancing the static characteristics. Reference [13] proposed a sensorless control strategy based on a nonlinear extended state observer for load torque compensation, which improved the system's ability to resist external disturbances across the entire speed range. Furthermore, reference [14] replaced the switch function with a sine saturation function and utilized a variable cutoff frequency and Kalman filter for secondary filtering of back electromotive force. This approach resulted in reduced speed error and improved system stability. In order to improve system oscillations, shorten response time, and enhance disturbance rejection performance, the above references provide several methods.

* Corresponding author: 2291214429@qq.com

However, it is important to note that each method has its own limitations.

This paper aims to enhance the performance of traditional Sliding Mode Control (SMC) by improving the exponential reaching law and selecting an integral sliding surface. The traditional sliding mode observer is enhanced by replacing the sign function with the sigmoid function and using a variable cutoff frequency filter to effectively filter various velocity segments. Additionally, an improved version of the Extended State Observer (ESO) is designed by incorporating the SMC law into the ESO and setting a variable cutoff frequency filter to enhance the accuracy of the ESO. The ESO estimates and feeds back unknown disturbances to the q-axis current, thereby compensating for disturbances and improving the system's disturbance rejection capability.

2 PMSM mathematical model

To facilitate the establishment of a mathematical model for PMSMs, it is assumed that the motor operates under ideal conditions. In the *d*-*q* axis coordinate system, the voltage equation for PMSMs is expressed as:

$$\begin{cases} u_d = Ri_d + L_d \dfrac{d}{dt} i_d - \omega_e L_q i_q \\ u_q = Ri_q + L_q \dfrac{d}{dt} i_q - \omega_e \left(L_d i_d + \varphi_f\right) \end{cases} \tag{1}$$

where the variables u_d and u_q represent the voltage components along the d and q axes respectively, while i_d and i_q represent the current components along the d and q axes. L_d and L_q are the inductance components along the d and q axes, respectively. R denotes the stator inductance. ϕ_d and ϕ_q represent the magnetic flux components along the d and q axes respectively, while ϕ_f represents the magnetic flux of the permanent magnet. Finally, ω_e represents the electrical angular velocity.

The electromagnetic torque expression of a PMSM is:

$$T_e = \frac{3}{2} p i_q \varphi_f \tag{2}$$

where T_e represents the electromagnetic torque, while p denotes the number of poles in the motor.

The mechanical motion expression of a PMSM is:

$$J \frac{d\omega_m}{dt} = T_{\mathrm{e}} - B\omega - T_{\mathrm{L}} \tag{3}$$

where the variable B represents the damping coefficient, ω denotes the mechanical angular velocity, which is defined as the ratio of ω_e to np. T_{L} signifies the load torque, J represents the moment of inertia, and T_e represents the electromagnetic torque.

3 Improving reaching law design

3.1 Traditional exponential reaching law

The concept of reaching law was initially proposed by the renowned academician Weibing Gao, who also developed the notion of exponential reaching law. The traditional form of exponential reaching law is as follows:

$$\dot{s} = -\varepsilon sign(s) - qs. \tag{4}$$

where the variable s represents the sliding mode function, while ε and q denote the approaching parameters, both being positive values. Additionally, the function *sign(s)* stands for the sign function.

The traditional exponential reaching law comprises a constant term, referred to as $sign(s)$, and an exponential term, denoted as $-qs$. When the moving point is far from the sliding surface, both the exponential term and the constant term contribute, with the exponential term being more significant. However, during the sliding motion of the moving point, the constant term becomes more prominent, and the exponential term tends to approach zero.

3.2 Fast exponential reaching law

To address the issue of oscillation in traditional exponential reaching laws and reduce response time, this paper presents an improved form of exponential reaching. The proposed method is as follows:

$$\begin{cases} \dot{s} = -\varepsilon D(s) sign(s) - q|X|^{\alpha} s. \\ D(s) = \dfrac{1}{e^{-|s|^b} + \frac{1}{|s|+a}} \end{cases} \tag{5}$$

where a, b, q and α, possess values that are greater than zero.

For SMC, the motion before reaching the sliding surface is called approach motion. By changing the ground parameters in the reaching law, the speed of the process can be guaranteed and the jitter phenomenon in the system can be attenuated.

The improved approach proposed in this paper introduces a function *D(s)* in the constant term and a power of the velocity error state variable $|X|$ in the exponential term. When the motion point is infinitely far from the sliding surface, $|s|$ tends to infinity, and *D(s)* also tends to infinity, thus further enhancing the convergence speed of the motion point. On the other hand, when the motion point is near the sliding surface, $|s|$ tends to zero, and *D(s)* is less than 1, resulting in a reduced convergence speed. The power of the velocity error state variable $|X|$ in the exponential term correlates the convergence speed with the variation of the system velocity error during the motion stage approaching the sliding mode switching surface. In comparison to traditional approaches, the improved approach not only shortens the system's response time but also effectively eliminates overshoot and reduces the magnitude of oscillation.

3.3 Analysis of the performance of Fast exponential reaching law

In order to conduct a comparative analysis, the following systems are established to examine the traditional exponential reaching law and the Fast exponential reaching law.

$$\ddot{\theta} = -f(\theta, t) + hu(t) \tag{6}$$

where $\theta(t)$ represents the position signal, $f(\theta,\ t) = 25\ \dot{\theta}(\mathrm{t})$, h is equal to 133, and $u(t)$ denotes the control input.

The error term $e(t)$ and its derivative are considered in this context:

$$\begin{cases} e(t) = \theta_d(t) - \theta(t) \\ \dot{e}(t) = \dot{\theta}_d(t) - \dot{\theta}(t) \end{cases} \tag{7}$$

where the variable $\theta_d(t)$ represents the ideal position signal.

The concept of the sliding mode function can be defined as follows:

$$s(t) = ce(t) + \dot{e}(t) \tag{8}$$

where the variable c represents a constant value that is greater than zero.

By equations (6)–(8), it can be derived that:

$$\dot{s}(t) = c\dot{e}(t) + \ddot{e}(t) = c\left(\dot{\theta}_d(t) - \dot{\theta}(t)\right) + \left(\ddot{\theta}_d(t) + f(\theta, t) - hu(t)\right). \tag{9}$$

By adopting a Fast exponential reaching law, equations (5) and (9) yield the following result:

$$u(t) = \frac{1}{h}\left[c\left(\dot{\theta}_d(t) - \dot{\theta}(t)\right) + \left(\ddot{\theta}_d(t) + f(\theta, t)\right) + \varepsilon D(s)sign(s) + q|X|^{\alpha}s\right]. \tag{10}$$

The simulation was conducted to compare the performance of the Fast exponential reaching law and the traditional exponential reaching law using the same set of parameters. The selected parameters were $c = 15$, $e = 10$, $q = 2$, $a = 2$, $b = 5$, $\alpha = 3$, and $X = x_1$. The ideal signal of the system, $\theta_d(t)$, was set to $\sin(t)$, and the initial state $x(0)$ was $[-2, -2]$. Figure 1 presents the performance comparison between the traditional exponential reaching law and the Fast exponential reaching law. From Figure 1, it can be observed that the Fast exponential reaching law outperforms the traditional exponential reaching law in terms of signal tracking, error convergence rate, and oscillation suppression. Therefore, it can be concluded that the proposed Fast exponential reaching law in this study can shorten the system response time and suppress system oscillations.

4. The design of the sliding mode velocity controller

4.1 The design of the velocity controller

The state variables of the PMSM control system are defined as follows:

$$\begin{cases} x_1 = \omega^* - \omega \\ x_2 = \int_{-\infty}^{t} (\omega^* - \omega)\mathrm{d}t \end{cases} \tag{11}$$

where ω^* represents the predetermined mechanical angular velocity of the motor, while ω denotes the actual mechanical angular velocity of the motor.

The integral sliding mode is to reasonably set the initial state of the integrator so that the initial state of the system is on the sliding surface at the beginning, it can reduce steady-state errors. Therefore, in this paper, the integral sliding surface is used instead of the traditional sliding surface. Equation (11) to define the function of the sliding surface as:

$$s = x_1 + cx_2. \tag{12}$$

Differentiating equation (11) yields:

$$\begin{cases} \dot{x}_1 = -\dfrac{3p\varphi_f}{2J} i_q + \dfrac{B}{J}\omega + \dfrac{1}{J} T_L \\ \dot{x}_2 = x_1 \end{cases}. \tag{13}$$

Differentiating equation (12) yields:

$$\dot{s} = \dot{\omega} + cx_1. \tag{14}$$

In the complex marine environment, the operation of PMSMs is affected by various uncertain disturbance factors. These disturbances can lead to changes in motor operating conditions, which in turn affect the load torque and the stability of motor operation. Therefore, it is crucial to measure the disturbance quantities during system disturbances.

Given the uncertainty of the parameters and external disturbances, we can substitute equation (2) into equation (3) and proceed with its rewriting.

$$\dot{\omega} = (d + \Delta d) i_q - (\eta + \Delta\eta)\omega - (c + \Delta c) T_L \tag{15}$$

where $d = \dfrac{3p\varphi_f}{2J}$; $\eta = \dfrac{B}{J}$; $c = \dfrac{1}{J}$. The values of Δd, $\Delta\eta$, and Δc are considered as the variables in this context $T_L = T_{L0} + \Delta T_L$.

The concept of comprehensive interference can be defined as:

$$g = \Delta d i_q - (\eta + \Delta\eta)\omega - (c + \Delta c) T_L. \tag{16}$$

Based on this inference, it can be concluded that:

$$\dot{\omega} = d i_q + g. \tag{17}$$

By substituting equations (5) and (17) into equation (14), the calculation yields:

$$d i_q + g + cx_1 = -\varepsilon D(s)sign(s) - q|x_1|^{\alpha}s. \tag{18}$$

When considering the variations in parameters and load torque, the expression for i_q can be derived according to equation (18).

$$i_q^* = \frac{1}{d}[cx_1 + g + \varepsilon D(s)sign(s) + q|x_1|^{\alpha}s]. \tag{19}$$

4.2 Stability analysis

The establishment of a Lyapunov function:

$$V = \frac{1}{2}s^2. \tag{20}$$

Upon taking the derivative with respect to the given variable, the following expression emerges:

$$\dot{V} = s\dot{s} = -\varepsilon s D(s) sign(s) - q|x_1|^{\alpha} s^2. \tag{21}$$

Given that ε is greater than 0, q is greater than 0, a is greater than 0, and b is greater than 0, it follows that $D(s)$ is greater than 0 and $s \cdot sign(s)$ is greater than 0. Consequently, $\dot{V}$ is less than 0, satisfying the accessibility condition.

5. The design of ESO based on SMC law

5.1 Enhancement of ESO Design

By considering the unknown disturbances existing in the offshore wind power system as expansion state variables of the system, the expansion state equation of the Extended State Observer (ESO) is designed as follows based on equation (17),

$$\begin{cases} \dot{\omega} = di_q + \mathrm{g} \\ \dot{g} = \chi(t) \end{cases} \tag{22}$$

where the symbol $\chi(t)$ represents the rate of change of an unknown perturbation g.

ESO is to define the external disturbance of the system and the uncertainty in the system as the expansion state variable for approximate estimation, and at the same time, the change of the system state variable can be quickly tracked, and the real-time correction and compensation can be carried out. For the PMSM control system, the dilated state observer expands the uncertain load torque and unknown disturbance into state variables and considers them as a whole for observation and estimation.

The design of the Extended State Observer (ESO) is characterized by the correlation between the estimated values of unknown disturbances and the SMC law. Additionally, the Linear Extended State Observer (LESO) enhances system accuracy by incorporating a function based on the SMC law into the observer.

$$\begin{cases} e_1 = z_1 - \omega \\ \dot{z}_1 = di_q + z_2 + \lambda_1 sgn(\hat{\omega} - \omega) \\ \dot{z}_2 = \beta_1 \lambda_1 sgn(\hat{\omega} - \omega) \end{cases} \tag{23}$$

where z_1 represents the estimated actual angular velocity of the motor, while z_2 denotes the estimated disturbance caused by g. λ_1 is a parameter of the Extended State Observer (ESO) and it is strictly less than zero. β_1 is another parameter of the ESO, and $\lambda_1 sgn(\hat{\omega} - \omega)$ stands for the SMC law.

The unknown disturbance estimation value, denoted by $\hat{g}$ in the system, is computed using equation (24) to determine the q-axis current required for the unknown disturbance and directly compensate it to the q-axis, thereby enhancing the disturbance rejection capability of the system.

$$i_{q,\mathrm{ESO}} = -\frac{\hat{g}}{d}. \tag{24}$$

Due to the presence of oscillation and discontinuity in traditional symbol functions, this paper utilizes the Sigmoid function as a replacement. The expression for the Sigmoid function is as follows:

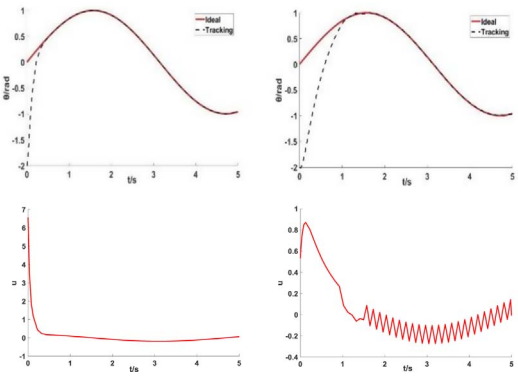

Fig. 1. Exponential reaching law performance comparison.

$$F(s) = \frac{2}{1 + e^{-\partial x}} - 1. \tag{25}$$

In this context, where $\partial > 0$ and as ∂ approaches infinity, the Sigmoid function tends to approximate the sign function.

In order to achieve more accurate filtering of the input signal, even in the presence of variations in velocity, a variable cutoff frequency filter is designed due to the inherent errors in the input signal of ESO. The mathematical expression representing this filter is as follows:

$$\begin{aligned} \hat{\omega}_c &= k_f \hat{\omega}_e + k_e \\ H(s) &= \frac{\hat{\omega}_c}{s + \hat{\omega}_c} \end{aligned} \tag{26}$$

where it is noted that the value of the parameter k_f is greater than zero, while the numerical value of k_e is relatively smaller (Fig. 2).

5.2 The analysis of errors in the ESO and the design of parameters

In order to investigate the errors of the ESO model, it is necessary to construct a dynamic equation that characterizes its error dynamics. The formulation for this equation is presented below:

$$\begin{cases} \dot{e}_1 = e_2 + \lambda_1 F(\hat{\omega} - \omega) \\ \dot{e}_2 = \beta_1 \lambda_1 F(\hat{\omega} - \omega) - \chi(t) \end{cases}. \tag{27}$$

When the stability condition is satisfied, as indicated by the following equation, e_1 approaches zero.

$$\begin{cases} (e_2 + \lambda_1) < 0, e_1 > 0 \\ (e_2 - \lambda_1) < 0, \quad e_1 > 0 \end{cases}. \tag{28}$$

The stable condition, denoted as $\lambda_1 < -|e_2|$, can be obtained by solving the equation. Moreover, when e_1 is equal to zero, equation (27) can be rewritten.

$$\begin{cases} e_2 = -\lambda_1 F(\hat{\omega} - \omega) \\ e_2 = \beta_1 \lambda_1 F(\hat{\omega} - \omega) - \chi(t) \end{cases}. \tag{29}$$

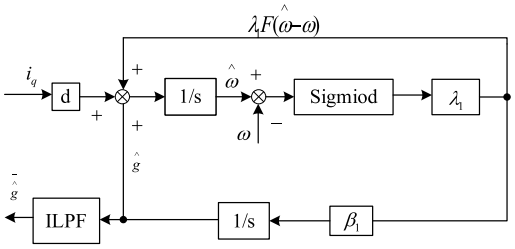

Fig. 2. The expansion state observer block diagram.

As deduced from the above equation,

$$\begin{cases} \dot{e}_2 + \beta_1 e_2 + \chi(t) = 0 \\ e_2 = e^{-\beta_1 t}[C_2 + \int \chi(t) e^{\beta_1 t} dt] \end{cases} \tag{30}$$

where C_2 represents a constant value.

According to equation (30), it can be inferred that the perturbation error will only converge to zero when β_1 is greater than zero.

6 The refinement of the sliding mode observer

6.1 The improved sliding mode observer

The improved SMO replaces the sign function with a smoother sigmoid function. Additionally, a variable cutoff frequency low-pass filter is used instead of the traditional filter. The inputs of the sliding mode controller are the voltage and current of the PMSM, while the outputs are the speed and angular position. The mathematical model of the sliding mode observer is established for the α and β axes as follows:

$$\frac{\mathrm{d}}{\mathrm{d}t}\begin{bmatrix} \hat{i}_\alpha \\ \hat{i}_\beta \end{bmatrix} = A\begin{bmatrix} \hat{i}_\alpha \\ \hat{i}_\beta \end{bmatrix} + \frac{1}{L_d}\begin{bmatrix} u_\alpha \\ u_\beta \end{bmatrix} - \frac{1}{L_d}\begin{bmatrix} z_\alpha \\ z_\beta \end{bmatrix} \tag{31}$$

where $\hat{i}_\alpha, \hat{i}_\beta$ represent the observed values of the stator current, while u_α, u_β signify the control inputs of the observer.

The equation for the stator current error can be expressed as follows:

$$\frac{\mathrm{d}}{\mathrm{d}t}\begin{bmatrix} \tilde{i}_\alpha \\ \tilde{i}_\beta \end{bmatrix} = A\begin{bmatrix} \tilde{i}_\alpha \\ \tilde{i}_\beta \end{bmatrix} + \frac{1}{L_d}\begin{bmatrix} e_\alpha - z_\alpha \\ e_\beta - z_\beta \end{bmatrix} \tag{32}$$

where $\tilde{i}_\alpha = \hat{i}_\alpha - i_\alpha, \tilde{i}_\beta = \hat{i}_\beta - i_\beta$ represent the errors in the observed current, $A = \frac{1}{L_d}\begin{pmatrix} -R & \\ & -R \end{pmatrix}$. The SMC law is designed as follows:

$$\begin{bmatrix} z_\alpha \\ z_\beta \end{bmatrix} = \begin{bmatrix} kF(\hat{i}_\alpha - i_\alpha) \\ kF(\hat{i}_\beta - i_\beta) \end{bmatrix} \tag{33}$$

where the symbol k represents the gain of the sliding mode observer.

Once the state variable reaches the sliding surface, it will initiate sliding motion. At this point, the following relationship holds:

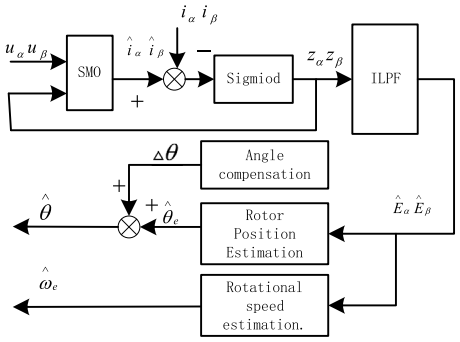

Fig. 3. The improved sliding mode observer diagram.

$$\begin{bmatrix} e_\alpha \\ e_\beta \end{bmatrix} = \begin{bmatrix} kF(\hat{i}_\alpha - i_\alpha) \\ kF(\hat{i}_\beta - i_\beta) \end{bmatrix}. \tag{34}$$

6.2 Estimating the position and velocity of a rotor

The estimated value of the counter-electromotive force after being filtered by a low-pass filter with a cut-off frequency can be determined by equations (26) and (34).

$$\begin{bmatrix} \hat{E}_\alpha \\ \hat{E}_\beta \end{bmatrix} = \begin{bmatrix} \dfrac{\hat{\omega}_c}{s + \hat{\omega}_c} e_\alpha \\ \dfrac{\hat{\omega}_c}{s + \hat{\omega}_c} e_\beta \end{bmatrix} \tag{35}$$

where $\hat{E}_\alpha, \hat{E}_\beta$ represent estimated counter-electromotive forces that have been filtered through a low-pass filter with a variable cut-off frequency.

Typically, the arctangent function is employed to obtain the rotor position.

$$\hat{\theta}_{\mathrm{eq}} = -\arctan(\hat{E}_\alpha / \hat{E}_\beta). \tag{36}$$

In order to address the issue of phase delay caused by the estimated component of counter-electromotive force obtained through a filter, which in turn affects the accuracy of estimating rotor position, it is necessary to incorporate an angular compensation term in the aforementioned equation.

$$\hat{\theta}_e = \hat{\theta}_{eq} + \arctan(\hat{\omega}_e / \omega_c). \tag{37}$$

The expression for estimating the rotational speed is as follows (Fig. 3):

$$\hat{\omega}_e = \frac{\sqrt{\hat{E}_\alpha^2 + \hat{E}_\beta^2}}{\varphi_f} \tag{38}$$

7 Simulation results and analysis

The control structure diagram for the LESO-based position sensorless control of a PMSM, as described in this article, is shown in Figure 4. The parameters of the PMSM can be found in Table 1. A system simulation model was developed using Matlab/Simulink. Comparative experiments were performed to evaluate the system's performance in terms

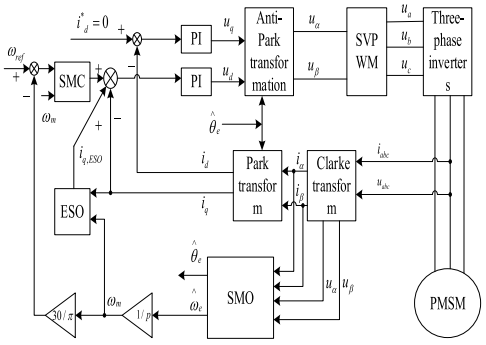

Fig. 4. The strategy control diagram in this paper.

Table 1. Motor parameters.

Parameter name	Parameter value
Stator inductance (L_s/mH)	8.5
Stator resistance (R/Ω)	2.875
Magnetic flux (φ_f/Wb)	0.175
Number of pole pairs (p)	4
Rotational inertia (j)	0.003
Damping coefficient (B)	0.008
DC voltage (U_{dc}/V)	311

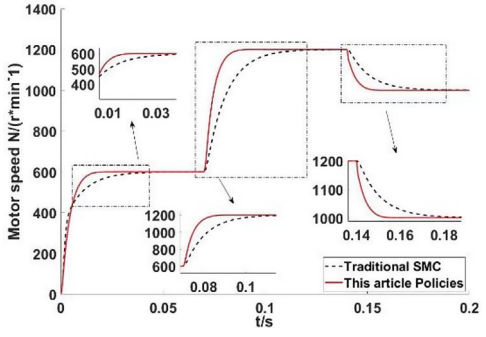

Fig. 5. Comparison of response under sudden changes in rotational speed.

of no-load start-up, sudden speed increase and decrease, and disturbance rejection capability.

1. The empty-load start-up process is illustrated in Figure 5, with a given start-up speed of 600 r min^{-1}. Within 0.07 s, the speed increases to 1200 r min^{-1}, and then abruptly drops to 1000 r min^{-1} at 0.14 s. A comparison of the results shows that the control system designed in this study exhibits superior response speeds in each stage compared to traditional SMC. Specifically, the response time in the first stage is 0.03 s faster than traditional sliding mode control, while in the second stage, it is 0.035 s faster, and in the third stage it is 0.04 s faster.

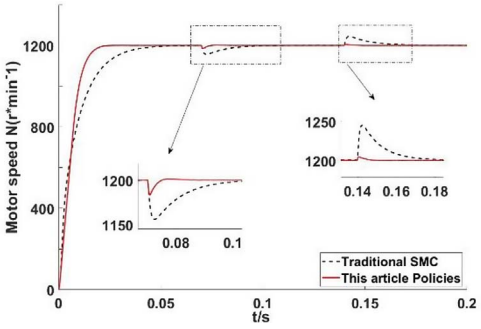

Fig. 6. The response to load variations is compared.

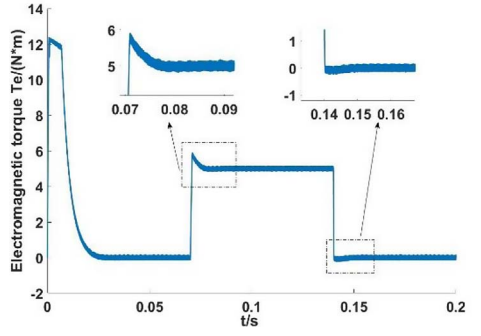

Fig. 7. The electromagnetic torque of control strategies in this article.

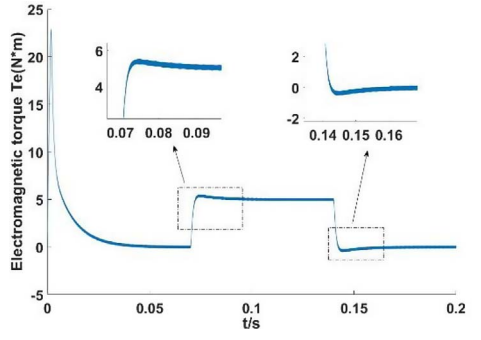

Fig. 8. Traditional SMC electromagnetic torque.

2. Given the target rotational speed of 1200 r min^{-1}, the load is suddenly increased to 5N m in 0.07 s and then decreased to 0 N m in 0.14 s. The comparative results are shown in Figures 6–9. During the sudden increase and decrease of the load in the system, the control strategy proposed in this paper demonstrates excellent disturbance rejection performance in terms of rotational speed, electromagnetic torque, and rotational speed error. Specifically, during the sudden increase of the load, the rotational speed disturbance is reduced by 27 r min^{-1} compared to the traditional sliding mode, and the response time is shortened by 0.036 s. Similarly, during the sudden decrease of the load, the rotational speed disturbance is reduced by 40 r min^{-1}, and the response time is shortened by 0.035 s.

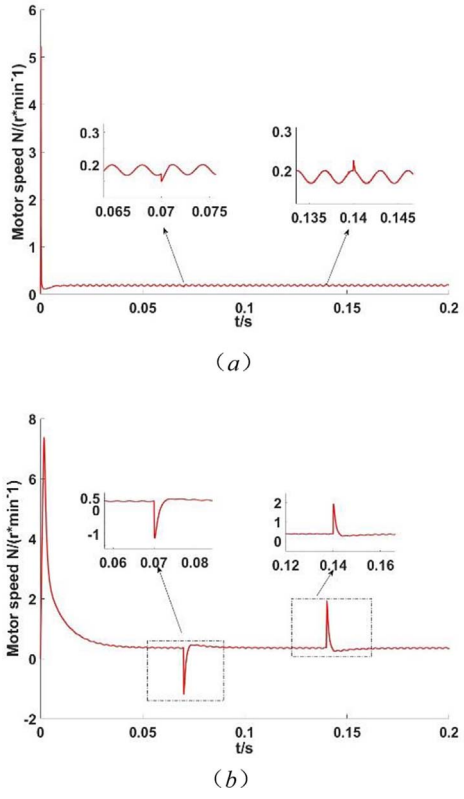

Fig. 9. Speed error comparison. a) The speed error control strategy in this text; b) Traditional SMC speed error.

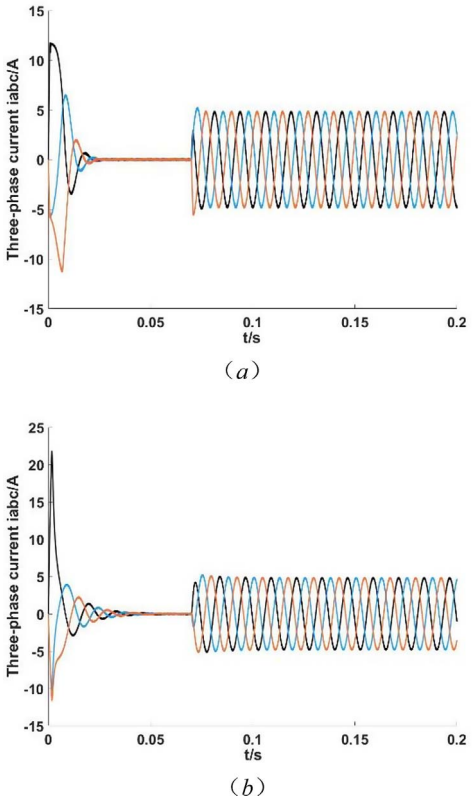

Fig. 10. Comparing the three-phase current with an additional load in 0.07 s. a) The three-phase current control strategy; b) The traditional three-phase current of SMC strategy.

The electromagnetic torque comparison of the two control methods is illustrated in Figures 7 and 8. When the motor starts, the electromagnetic torque of the control strategy proposed in this paper is reduced, resulting in a shorter time required to reach a steady state. Moreover, in the presence of external disturbances, the response speed is faster than that of the traditional SMC, indicating a significant improvement in disturbance rejection performance.

The comparison of speed error between the two control methods is illustrated in Figure 9. It is evident that the speed error fluctuations in different time periods of the motor are smaller with the control strategy proposed in this paper compared to the conventional SMC.

Figure 10 presents a comparison of the three-phase currents between two control strategies. It is evident that the proposed control strategy exhibits a lower starting current and significantly reduced settling time compared to the conventional SMC.

8 Conclusion

In order to improve the problems of slow response speed and poor anti-interference ability faced by the pitch motor in practice, the traditional SMC strategy was improved. On the basis of the traditional exponential reaching law, the fast exponential reaching law is designed, which not only improves the jitter of the moving point on the sliding mode surface but also accelerates the response speed. In addition, in order to solve the influence of disturbance on the efficiency of pitch motors, an ESO with SMC law is designed. ESO is used to observe interference and carry out feedforward compensation, and compared with the traditional control strategy, the proposed control strategy combines ESO feedforward compensation with SMC to improve the performance of the speed control system. It reduces the velocity error, improves the accuracy of the observer, and exhibits good anti-interference ability. This strategy can meet the challenges of the complex offshore environment and improve the efficiency of pitch motors. In addition, it is necessary to increase the full consideration of the complex offshore environment to ensure the perfection of the control strategy.

References

1 Wang Y., Zhu Y., Feng Y., Tian B. (2021) New reaching sliding mode control strategy of permanent magnet synchronous motor, *Elect. Power Autom. Equip.* **41**, 01, 192–198.
2 Wang S., Fan C., Xu Q. (2022) New sliding mode variable structure control strategy of permanent magnet synchronous motor speed regulation system, *Automot. Technol.* **556**, 01, 1–7.
3 Amr I. (2022) Wind turbine blade dynamics simulation under the effect of atmospheric turbulence, *Emerg. Sci. J.* **7**, 1, 162–176.
4 Zhang L., Li X., Song P., Zhang P., Yun L. (2019) Sensorless vector control system of permanent magnet synchronous motor based on

new sliding mode observer, *Trans. China Electrotech. Soc.* **34**, 201, 70–78.
5 Liu J., Xiao F., Shen Y., Mai Z., Li C. (2017) Review of positionless sensor control technology of permanent magnet synchronous motor, *Trans. China Electrotech. Soc.* **32**, 16, 76–88.
6 Li Z., Hu G., Cui J., Liu G. (2014) Integral sliding mode variable structure control of permanent magnet synchronous motor speed regulation system, *Proc. CSEE* **34**, 03, 431–437.
7 Xia X., Zhang B., Li X., Zhang S. (2019) Low-speed sliding mode control of permanent magnet synchronous motor based on extended state observer, *Opt. Precis. Eng.* **27**, 12, 2628–2638.
8 Dong L. (2017) Research on sensorless stable performance control of electric vehicle motor, *Comput. Simul.* **34**, 5, 182–186.
9 Sun Q., Zhu X., Niu F. (2022) Sensorless control of permanent magnet synchronous motor based on new sliding mode observer with single resistor current reconstruction, *CES Trans. Electr. Mach. Syst.* **6**, 4, 378–383.
10 Chen Z., Xue Z., Fang H., Luo G. (2019) Speed regulation system of permanent magnet synchronous motor based on adaptive inverse control, *J. Northwest. Polytech. Univ.* **37**, 04, 824–829.
11 Yuan L., Jiang Y., Xiong L., Wang P. (2023) Sliding mode control approach with integrated disturbance observer for PMSM speed system, *CES Trans. Electr. Mach. Syst.* **7**, 1, 118–127.
12 Yuan S., Chen J., Zhou Y. (2021) Improved integral sliding mode structure design based on extended state observer, *Transducers Microsys.* **40**, 06, 107–109.
13 Wu C., Fu Z., Sun M., Liu Z. (2020) Position sensorless control of permanent magnet synchronous motor in full speed range based on load torque compensation of extended state observer, *Trans. China Electrotech. Soc.* **35**, S1, 172–181.
14 Chen J., Chi C. (2019) Research on sliding mode observer of permanent magnet synchronous motor based on sinusoidal saturation function, *Comb. Mach. Tool Auto. Proc. Technol.* **541**, 03, 67–70.